Monthly Notices of the ROYAL ASTRONOMICAL SOCIETY

MNRAS **516,** 550–561 (2022) https://doi.org/10.1093/mnras/stac2216
Advance Access publication 2022 August 6

An *ab initio* study for the photodissociation of HCl and HF

Zhi Qin [1,2] Tianrui Bai[1,2] and Linhua Liu [1,2,3]★

[1]*Optics and Thermal Radiation Research Center, Institute of Frontier and Interdisciplinary Science, Shandong University, Qingdao, Shandong 266237, China*
[2]*School of Energy and Power Engineering, Shandong University, Jinan 250061, China*
[3]*School of Energy Science and Engineering, Harbin Institute of Technology, Harbin 150001, China*

Accepted 2022 August 2. Received 2022 August 1; in original form 2022 June 19

ABSTRACT

Detailed studies of HCl and HF photodissociation are required for an in-depth understanding the chlorine and fluorine chemistry in Venus and exoplanets. Here, we present an *ab initio* study of photodissociation of HCl and HF. Except for the widely studied A $^1\Pi \leftarrow$X $^1\Sigma^+$ photodissociation process, the ground-state photodissociation processes for HCl and HF via higher excited states are considered. State-resolved cross-sections are computed for nine photodissociation processes of HCl from a total of 871 ground rovibrational levels. For HF, seven photodissociation processes are considered for the computation of state-resolved cross-sections from all the rovibrational levels in the ground state. Subsequently, temperature-dependent cross-sections for the considered transition processes of HCl and HF are estimated from 0 to 10 000 K with a grid of 34 temperatures. Careful comparisons with the recent ExoMol study and the Leiden Observatory database are made. The photodissociation rates in the interstellar and blackbody radiation fields are also discussed.

Key words: astrochemistry – molecular data – molecular processes.

1 INTRODUCTION

HF and HCl are members of the hydrogen halide family HX (X = F, Cl, Br, I) and are often used as a benchmark for the study of fundamental physical phenomena. As an example, HF and HCl provide excellent molecular systems for investigating the photodissociation phenomena, which is a key photochemical process in many ultraviolet (UV)-rich astrophysical environments. HCl and HF were detected in the interstellar medium (Smith et al. 1980; Indriolo et al. 2013; Monje et al. 2013) and in the coma of comet 67P/Churyumov–Gerasimenko (De Keyser et al. 2017; Dhooghe et al. 2017). HCl was also observed in the atmosphere of some solar planets such as Venus (Yung & DeMore 1982; Bahou et al. 2001; Sandor & Clancy 2012). Photodissociation of HCl and HF is the principal destruction process in the interstellar medium and plays a major role in the atmospheric evolution of Venus, and has therefore been investigated continuously since 1930s.

Photodissociation cross sections are important parameters for determining the abundances of interstellar molecules, such as HeH^+ (Miyake, Gay & Stancil 2011), SH^+ (McMillan et al. 2016), MgO (Bai, Qin & Liu 2021), AlF (Qin, Bai & Liu 2022), CO_2 (Grebenshchikov 2016), HCl, and HF (Valiev et al. 2020), or understanding the chemical evolution in clouds, envelopes, and discs (Heays, Bosman & van Dishoeck 2017). Measurements of photodissociation cross sections had been performed for HCl (Myer & Samson 1970; Inn 1975; Nee, Suto & Lee 1986; Cheng et al. 2002; Brion, Dyck & Cooper 2005) and HF (Hitchcock et al. 1984; Nee, Suto & Lee 1985). In these experiments, the double-beam absorption spectrometer (Myer & Samson 1970), the electron energy-loss method (Hitchcock et al. 1984), and the synchrotron radiation (Nee, Suto & Lee 1985, 1986; Cheng et al. 2002; Brion et al. 2005) were used. From a theoretical point of view, the quantum mechanical technique was often chosen to investigate the photodissociation of HCl and HF. For instance, van Dishoeck, van Hemert & Dalgarno (1982) adopted the multireference single- and double-excitation configuration interaction (MRD-CI) method to evaluate the transition of HCl by absorption of energy into the A $^1\Pi$ state, resulting in photodissociation, and by absorption of energy into the bound C $^1\Pi$ state, followed by pre-dissociation. An upper limit for the photodissociation rate of HCl was also determined. The same (MRD-CI) method with Davidson correction was utilized by Cacelli (1996) to compute the photoabsorption cross section of HF resulting from the A $^1\Pi \leftarrow$X $^1\Sigma^+$ transition. In addition, Brown & Balint-Kurti (2000a,b) carried out a time-dependent wave packet study for the spin–orbit branching in the photodissociation of HF and DF.

All these studies about the cross sections of HCl and HF take no account of the temperature dependence, nor did they consider the effects of rovibrational excitations. Therefore, this work aims to produce the temperature-dependent photodissociation cross sections and rates of HCl and HF from the rovibrational excitations in their ground state, which are vital to modelling the chemistry of atmospheres in planets such as Venus or some hot exoplanets. The quantum mechanical method is used, in which potential energy curves (PECs) and transition dipole moments (TDMs) are basic input data. The *ab initio* study of HCl was carried out by Engin, Sisourat & Carniato (2012), who presented a large number of electronic states of this molecule at a post-Hartree–Fock configuration interaction level of theory including up to quadruple electronic excitations (CI-SDTQ). They presented high-level *ab initio* PECs and TDMs, as well as visible/UV absorption spectrum and absolute optical oscillator strengths. More recently, Liu et al.

★ E-mail: liulinhua@sdu.edu.cn

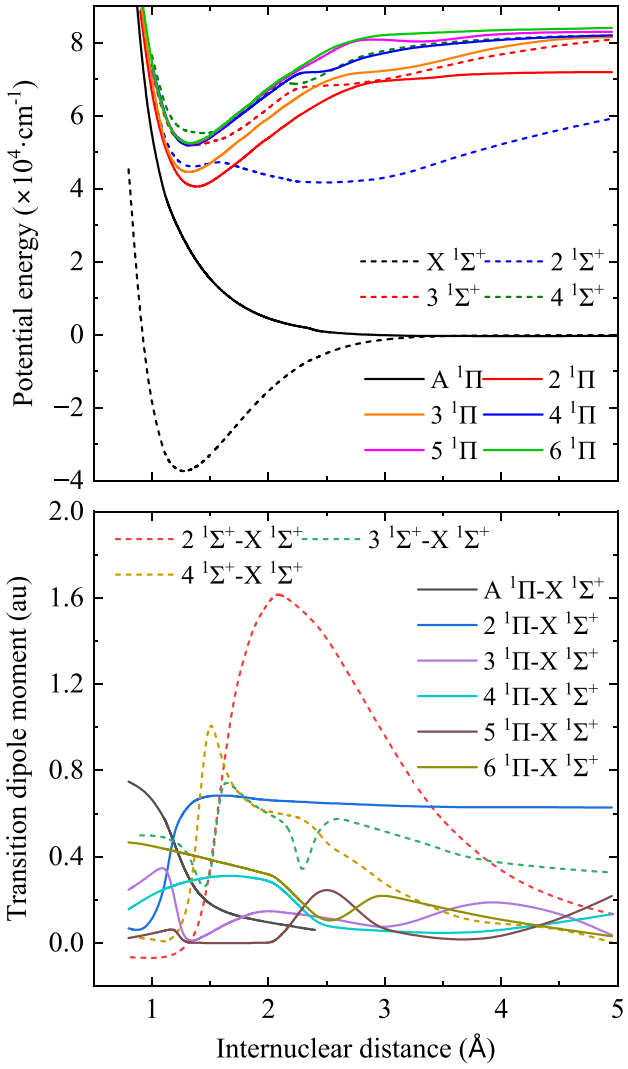

Figure 1. Potential energy curves and transition dipole moments for HCl. PECs of the X $^1\Sigma^+$ and A $^1\Pi$ states and their TDM are calculated in this work. The other PECs and TDMs are taken from Engin et al. (2012).

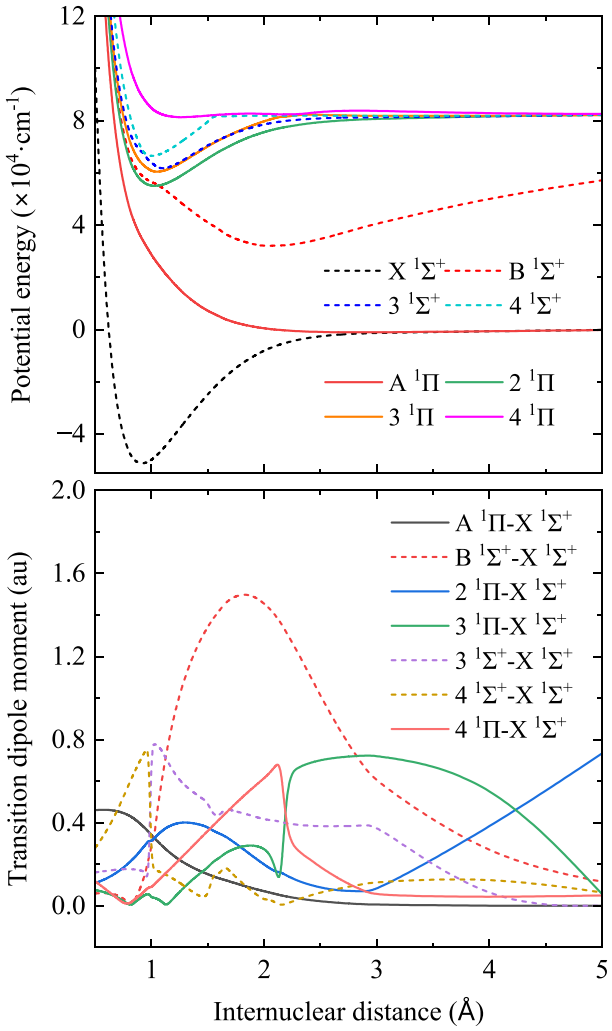

Figure 2. Potential energy curves and transition dipole moments for HF. All the PECs and TDMs are taken from Liu et al. (2021).

(2021) carried out high-level *ab initio* study of HF by the multireference configuration interaction method plus Davidson correction (MRCI+Q) and presented the PECs and TDMs of HF. We have adopted these *ab initio* PECs and TDMs from Engin et al. (2012) and Liu et al. (2021) for this study on the photodissociation of HCl and HF, respectively. Note that the ExoMol group provided a similar calculation of photodissociation cross sections and rates of HCl and HF (Pezzella, Tennyson & Yurchenko 2022). Careful comparisons with their results are made in this work.

This work is organized as follows. The theory and method for the calculation of photodissociation cross sections and rates are given in Section 2, as well as the adopted PECs and TDMs. The corresponding results and discussions are presented in Section 3. In Section 4, the concluding remarks are drawn.

2 THEORY AND METHOD

2.1 PECs and TDMs

To obtain the cross sections detailed below, we used *ab initio* PECs and TDMs of HCl from Engin et al. (2012) except for the PECs of the X $^1\Sigma^+$ and A $^1\Pi$ states and their TDM, which are calculated by the MRCI+Q method with the aug-cc-pCV5Z-DK basis set for Cl and the aug-cc-pV5Z-DK basis set for H, as shown in Fig. 1. For HF, a recent set of PECs and TDMs was taken from Liu et al. (2021), as shown in Fig. 2. Engin et al. (2012) reported the PECs and TDMs of HCl for internuclear distances from $R = 0.8$ to 5 Å, and Liu et al. (2021) provided the PECs and TDMs for the range of internuclear distances from 0.4 to 5 Å. For R larger than 5 Å, the PECs were extrapolated to the long-range behaviours by

$$V(R) = -\frac{C_5}{R^5} - \frac{C_6}{R^6} + V(R \to \infty), \quad (1)$$

where C_5 and C_6 are fitting coefficients and are approximately evaluated in this work. C_6 can be estimated by the London formula (London 1937), given by

$$C_6 = \frac{3}{2}\frac{\Gamma_H \Gamma_X}{\Gamma_H + \Gamma_X}\alpha_H \alpha_X \,(\mathrm{X} = \mathrm{Cl} \quad \text{or} \quad \mathrm{F}), \quad (2)$$

where Γ is the ionization energy for a given atomic state, which can be obtained from NIST Atomic Spectra Database (Kramida et al. 2021). α is the static dipole polarizability for a specific electronic state. $\alpha = 4.4962$ au from the CCSD(T) calculation is chosen for the ground H ($1s\ ^2$S) state (Wang et al. 2021). For the ground state Cl

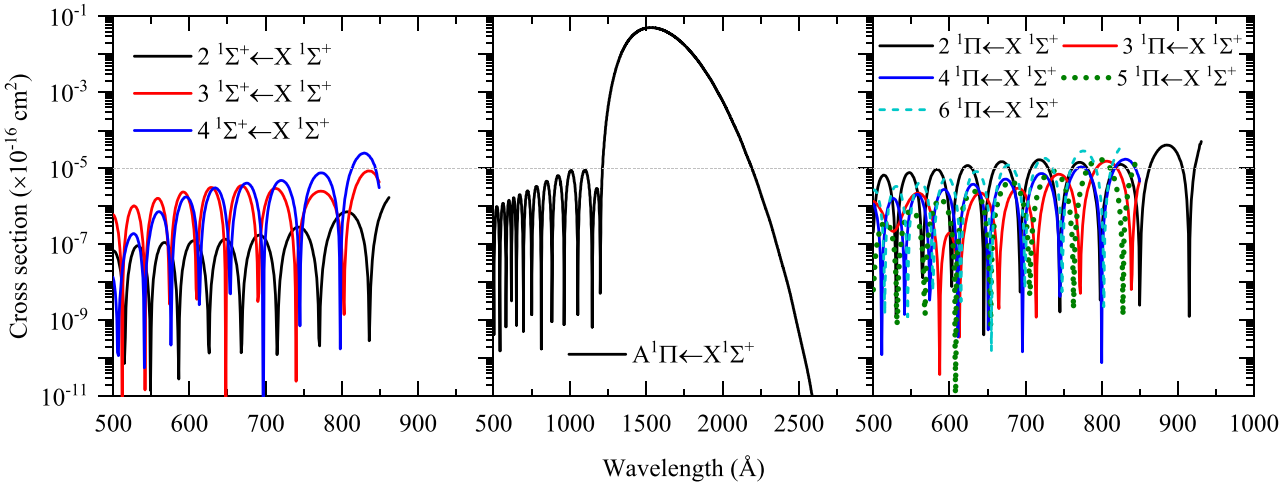

Figure 3. State-resolved photodissociation cross sections for nine electronic transitions of HCl from the ground rovibrational level $(\upsilon'', J'') = (0, 0)$.

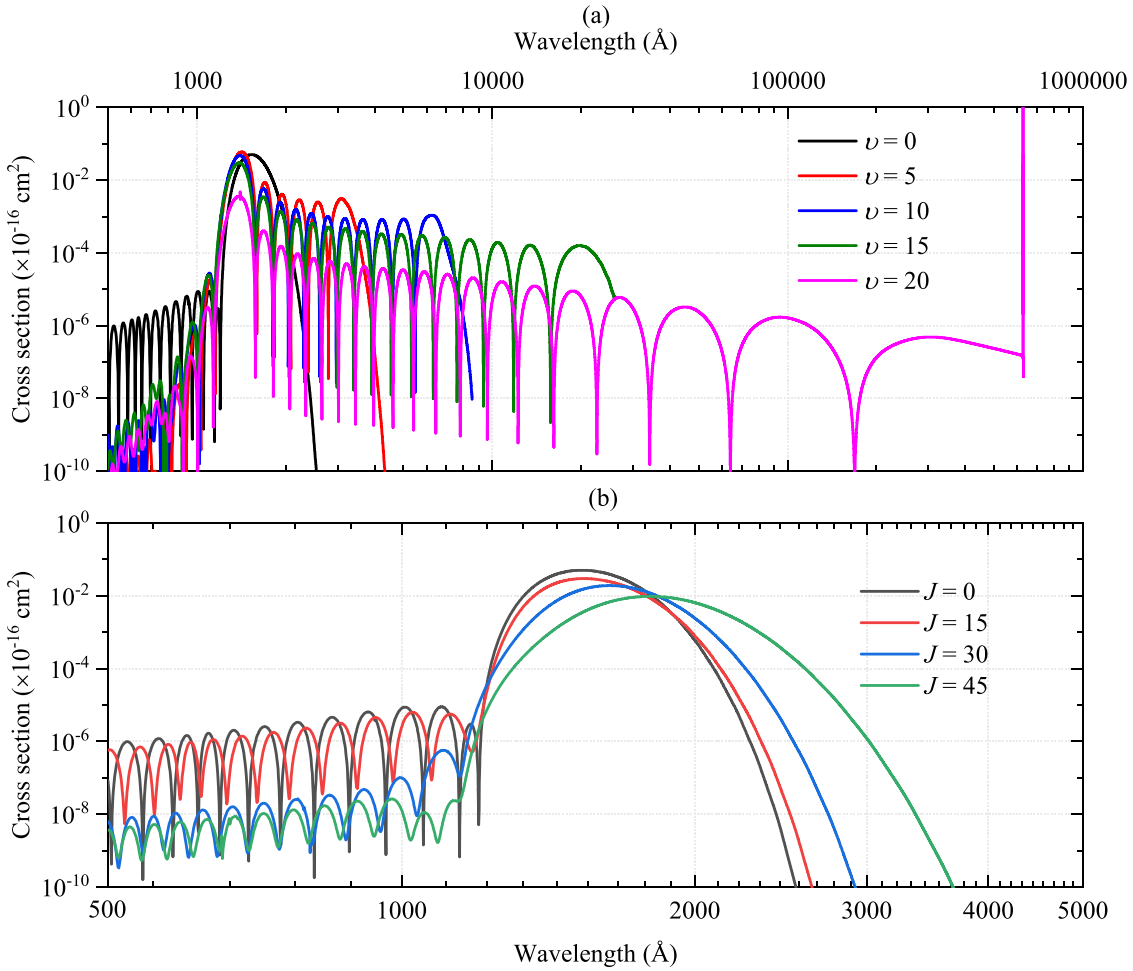

Figure 4. The computed state-resolved photodissociation cross sections of HCl for the A $^1\Pi \leftarrow$X $^1\Sigma^+$ transition from initial rovibrational levels (a) where $J'' = 0$ and $\upsilon'' = 0$, 5, 10, 15, and 20 and (b) where $\upsilon'' = 0$ and $J'' = 0$, 15, 30, and 45.

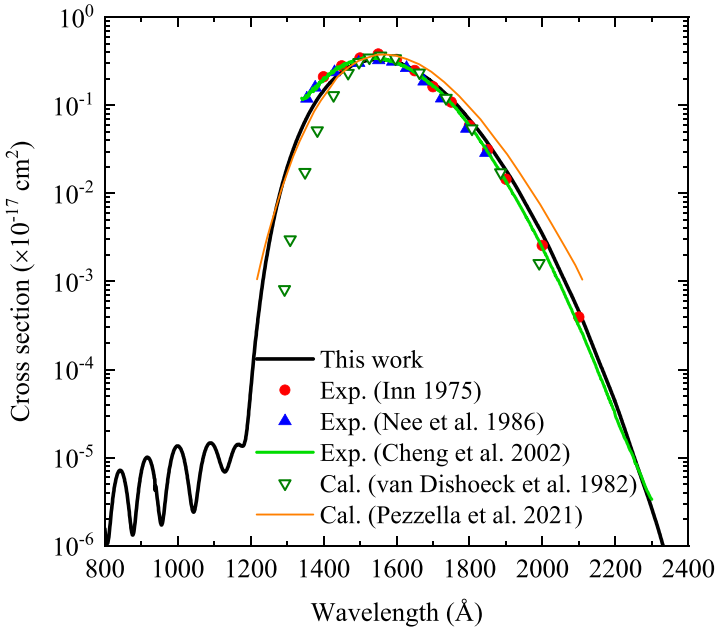

Figure 5. Comparison of the photodissociation cross sections of the HCl A $^1\Pi \leftarrow$X $^1\Sigma^+$ transition with the experimental data from Inn (1975) and Cheng et al. (2002) and theoretical ones calculated by van Dishoeck et al. (1982) and Pezzella et al. (2021). The present calculations are performed at 100 K.

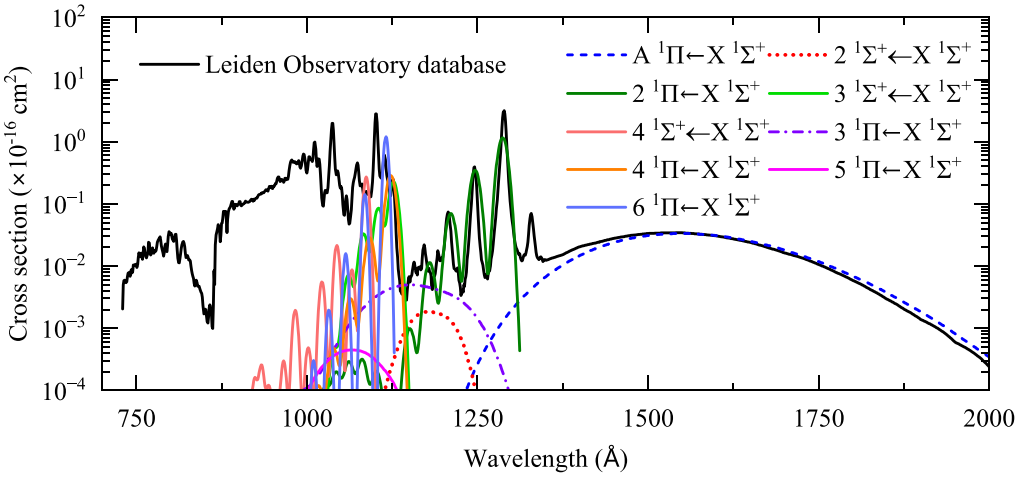

Figure 6. Photodissociation cross sections of HCl for nine electronic transitions at 0 K. The total spectrum is composed of a continuum band of the A $^1\Pi \leftarrow$X $^1\Sigma^+$ transition at wavelengths larger than about 1300 Å, a discrete progression of 2 $^1\Pi \leftarrow$X $^1\Sigma^+$ at wavelengths about 1150–1300 Å, and another set of discrete transitions of 3 $^1\Sigma^+ \leftarrow$X $^1\Sigma^+$, 4 $^1\Sigma^+ \leftarrow$X $^1\Sigma^+$, 4 $^1\Pi \leftarrow$X $^1\Sigma^+$, and 6 $^1\Pi \leftarrow$X $^1\Sigma^+$ at wavelengths about 1040–1150 Å. The contributions of other transitions are insignificant. Note that the peaks of discrete transitions depend greatly on the Gaussian smoothing function, while the integrated cross sections are conserved. The cross sections are compared with the experimental data collected in Leiden Observatory database (Heays et al. 2017).

($3s^2 3p^5\,^2$P), $\alpha = 14.593$ au is selected from Wang et al. (2021). And $\alpha = 3.68$ au is adopted for the ground F ($2s^2 2p^5\,^2$P) state (Wang et al. 2021). For the excited states of H and Cl, the dipole polarizability for each one is chosen to be the same value as its corresponding ground state. To ensure the smoothness of PECs around the extrapolation region, C_5 are estimated by fitting *ab initio* points while keeping the dissociation limits and C_6 fixed. For the short-range behaviour down to 0.3 Å, the PECs were extrapolated by the following function:

$$V(R) = A\exp(-BR) + C, \tag{3}$$

where A, B, and C are fitting parameters. For TDMs, the long-range and short-range behaviours are also fitted using equations (1) and (3), respectively. Such treatment of extrapolation was also adopted for other diatomic molecules (el-Qadi & Stancil 2013; Qin, Bai & Liu 2021a; Bai, Qin & Liu 2022).

2.2 Photodissociation cross-sections and rates

The photodissociation cross section for a bound–free transition from an initial state i to a final state f can be given by the following relationship:

$$\sigma^{fi}\left(E_{\rm ph}\right) = \frac{4\pi^2}{3}\alpha E_{\rm ph}\left|\left\langle \Phi_f(\boldsymbol{r},\boldsymbol{R})\left|\boldsymbol{r}\right|\Phi_i(\boldsymbol{r},\boldsymbol{R})\right\rangle\right|^2, \tag{4}$$

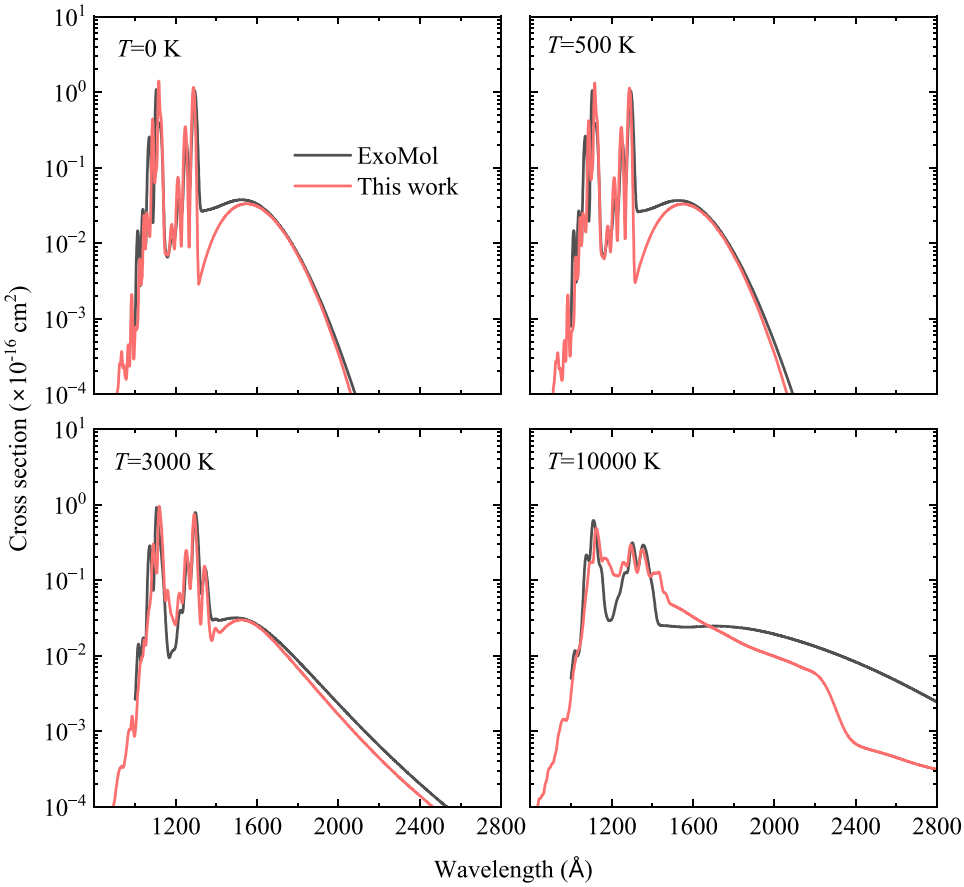

Figure 7. Comparison of the total photodissociation cross section of HCl with that from ExoMol group (Pezzella et al. 2022).

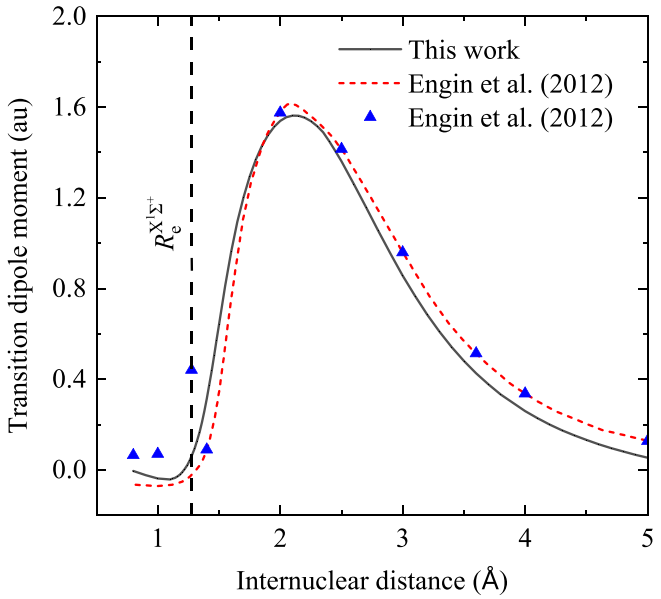

Figure 8. Transition dipole moment of $2\,^1\Sigma^+ \leftarrow X\,^1\Sigma^+$. The solid line is from this work. The dashed line is from fig. 3 in the paper of Engin et al. (2012). The symbols represent the values given in table IV of the paper from Engin et al. (2012).

where $\boldsymbol{r}$ is the vector of electronic coordinate, $\boldsymbol{R}$ is the vector of internuclear distance, $\Phi(\boldsymbol{r}, \boldsymbol{R})$ is the total molecular wavefunction, $E_{\rm ph}$ is the photon energy, and α is the fine-structure constant. The Born–Oppenheimer approximation separates Φ into the variables for the electronic and nuclear coordinates, and the electric dipole transition moment function can then be given by

$$D^{fi}(R) = \left\langle \phi_f(\boldsymbol{r}|R)\,|\boldsymbol{r}|\,\phi_i(\boldsymbol{r}|R)\right\rangle, \tag{5}$$

where $\phi(\boldsymbol{r}|R)$ is the electronic wavefunction for a fixed R and the integration is taken over all the r. Considering the rovibrational excitations, the state-resolved cross section for a transition from the rovibrational level $\upsilon''J''$ of the initial bound electronic state i to the continuum $k'J'$ of the final repulsive electronic state f can be written as

$$\sigma^{fi}_{\upsilon''J''}(E_{\rm ph}) = \frac{4\pi^2 e^2}{3\hbar c} E_{\rm ph}\, g \sum_{J'} \times \left(\frac{1}{2J''+1} S_{J'}(J'') \left|\left\langle \chi_{k'J'}(R)\left|D^{fi}(R)\right|\chi_{\upsilon''J''}(R)\right\rangle\right|^2\right), \tag{6}$$

where e is electron charge, $\hbar$ is the reduced Planck constant, c is the speed of light in vacuum, g is the degeneracy factor, $S_{J'}(J'')$ is the Hönl–London factor and its expression depends on different transition types (Hansson & Watson 2005; Watson 2008). The singlet transitions are considered in this work and the corresponding Hönl–London factors are detailed in previous publications (Hansson & Watson 2005; Qin, Bai & Liu 2021b,c). $\chi_{k'J'}(R)$ is the continuum

Table 1. Photodissociation rates (s^{-1}) of HCl under the standard ISRF at several temperatures.

Transition	0 K	500 K	1000 K	2000 K	3000 K	5000 K	10 000 K
$2\,^1\Sigma^+ \leftarrow X\,^1\Sigma^+$	2.69×10^{-12}	2.80×10^{-12}	3.30×10^{-12}	7.90×10^{-12}	2.01×10^{-11}	7.51×10^{-11}	3.05×10^{-11}
$3\,^1\Sigma^+ \leftarrow X\,^1\Sigma^+$	8.49×10^{-11}	8.45×10^{-11}	8.38×10^{-11}	8.29×10^{-11}	8.51×10^{-11}	9.84×10^{-11}	1.36×10^{-10}
$4\,^1\Sigma^+ \leftarrow X\,^1\Sigma^+$	4.10×10^{-11}	4.26×10^{-11}	4.67×10^{-11}	6.72×10^{-11}	9.31×10^{-11}	1.36×10^{-10}	1.91×10^{-10}
$A\,^1\Pi \leftarrow X\,^1\Sigma^+$	2.06×10^{-10}	2.03×10^{-10}	1.99×10^{-10}	1.95×10^{-10}	1.90×10^{-10}	1.80×10^{-10}	1.42×10^{-10}
$2\,^1\Pi \leftarrow X\,^1\Sigma^+$	5.08×10^{-10}	5.11×10^{-10}	5.14×10^{-10}	5.20×10^{-10}	5.26×10^{-10}	5.37×10^{-10}	5.56×10^{-10}
$3\,^1\Pi \leftarrow X\,^1\Sigma^+$	1.27×10^{-11}	1.23×10^{-11}	1.20×10^{-11}	1.30×10^{-11}	1.46×10^{-11}	1.74×10^{-11}	2.11×10^{-11}
$4\,^1\Pi \leftarrow X\,^1\Sigma^+$	8.01×10^{-11}	8.03×10^{-11}	8.06×10^{-11}	8.15×10^{-11}	8.26×10^{-11}	8.51×10^{-11}	8.84×10^{-11}
$5\,^1\Pi \leftarrow X\,^1\Sigma^+$	6.01×10^{-13}	5.82×10^{-13}	5.67×10^{-13}	5.81×10^{-13}	6.04×10^{-13}	6.44×10^{-13}	1.55×10^{-12}
$6\,^1\Pi \leftarrow X\,^1\Sigma^+$	1.67×10^{-10}	1.67×10^{-10}	1.67×10^{-10}	1.67×10^{-10}	1.66×10^{-10}	1.65×10^{-10}	1.58×10^{-10}
Total	1.10×10^{-9}	1.10×10^{-9}	1.11×10^{-9}	1.14×10^{-9}	1.18×10^{-9}	1.29×10^{-9}	1.32×10^{-9}

wavefunction for the final electronic state f, $\chi_{\upsilon'' J''}(R)$ is the bound rovibrational wavefunction for the initial electronic state i. $\chi_{k' J'}(R)$ and $\chi_{\upsilon'' J''}(R)$ were obtained by solving the radial Schrödinger equation using the renormalized Numerov method (Johnson 1977, 1978) with a step size of 0.001 Å over internuclear distances from 0.3 to 50 Å.

In local thermodynamic equilibrium (LTE), a Boltzmann distribution is assumed for the population of rovibrational levels of the electronic ground state. The LTE cross section can be then expressed as a function of both temperature T and wavelength λ:

$$\sigma(\lambda, T) = \frac{\sum_{\upsilon'' J''} (2J''+1) \exp(-|E_{\upsilon'' J''} - E_{00}|/k_B T)\, \sigma^{\rm fi}_{\upsilon'' J''}}{Q(T)}, \quad (7)$$

where $E_{\upsilon'' J''}$ is the energy of the rovibrational level $\upsilon'' J''$, k_B is the Boltzmann constant, and $Q(T)$ is the rovibrational partition function, given by

$$Q(T) = \sum_{\upsilon'' J''} (2J''+1) \exp(-|E_{\upsilon'' J''} - E_{00}|/k_B T). \quad (8)$$

In astrophysical applications, photodissociation rates are often used to model the abundance and evolution of species in space and can be computed by

$$k = \int \sigma(\lambda)\, I(\lambda)\, {\rm d}\lambda, \quad (9)$$

where $\sigma(\lambda)$ is the photodissociation cross section mentioned above and $I(\lambda)$ is the intensity for a radiation field. There are several standard UV radiation fields appropriate for various astrophysical environments. Here we focus on the widely used interstellar radiation field (ISRF) and blackbody radiation field. The wavelength-dependent intensity for the ISRF has been fitted to the following formula, given by

$$I(\lambda) = 3.2028 \times 10^{13} \lambda^{-3} - 5.1542 \times 10^{15} \lambda^{-4} + 2.0546 \times 10^{17} \lambda^{-5}. \quad (10)$$

This formula is valid for wavelengths between 91.2 and 200 nm. Later, the intensity for ISRF was extended to 2000 nm by van Dishoeck & Black (1982),

$$I(\lambda) = 3.67 \times 10^{4} \lambda^{0.7}. \quad (11)$$

For a blackbody radiation field, its intensity can be given by

$$I(\lambda, T_{\rm rad}) = \frac{8\pi c/\lambda^4}{\exp(hc/k_B T_{\rm rad}\lambda) - 1}, \quad (12)$$

where h is the Planck constant, $h = 6.626 \times 10^{-34}$ (J·s). k_B is the Boltzmann constant, $k_B = 1.381 \times 10^{-23}$ (J·K^{-1}). $T_{\rm rad}$ is the temperature of the blackbody. Followed previous works from Heays et al. (2017) and Pezzella et al. (2022), we consider the blackbodies of three different temperatures to describe different types of stars. The blackbody of $T_{\rm rad} = 4000$ K is used to model T Tauri stars and stars formed in the early stages (Appenzeller & Mundt 1989; Natta 1993). The blackbody of $T_{\rm rad} = 10\,000$ K is chosen to model the Herbig Ae stars and young A stars still embedded in gas dust envelope (Vioque et al. 2018). The blackbody of $T_{\rm rad} = 20\,000$ K is adopted to model the bright and short-living B stars (Habets & Heintze 1981). Note that the blackbody radiation fields are required to be normalized to match the energy intensity of the ISRF between 91.2 and 200 nm (Heays et al. 2017; Pezzella et al. 2022).

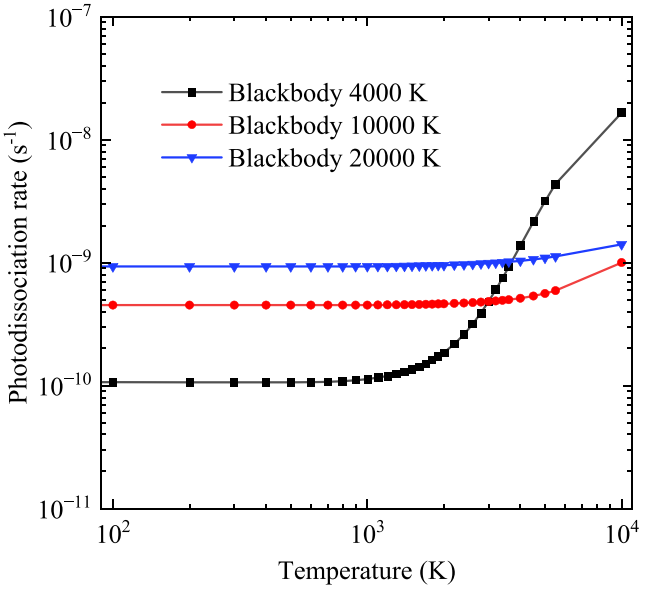

Figure 9. Photodissociation rates of HCl in the blackbody radiation fields of 4000 K (in black), 10 000 K (in red), and 20 000 K (in blue). The blackbody of 4000 K increases the rate by a factor of 165 from 100 to 10 000 K. The rates obtained using the blackbodies of 10 000 and 20 000 K do not show significant changes, with factors of 2.2 and 1.5, respectively.

3 RESULTS AND DISCUSSION

Based on the theory given above, we calculate the state-resolved and LTE cross sections, as well as the photodissociation rates for the HCl and HF. Except for the A $^1\Pi \leftarrow X\,^1\Sigma^+$ electronic transition, other electronic transitions from the ground state to the excited states are

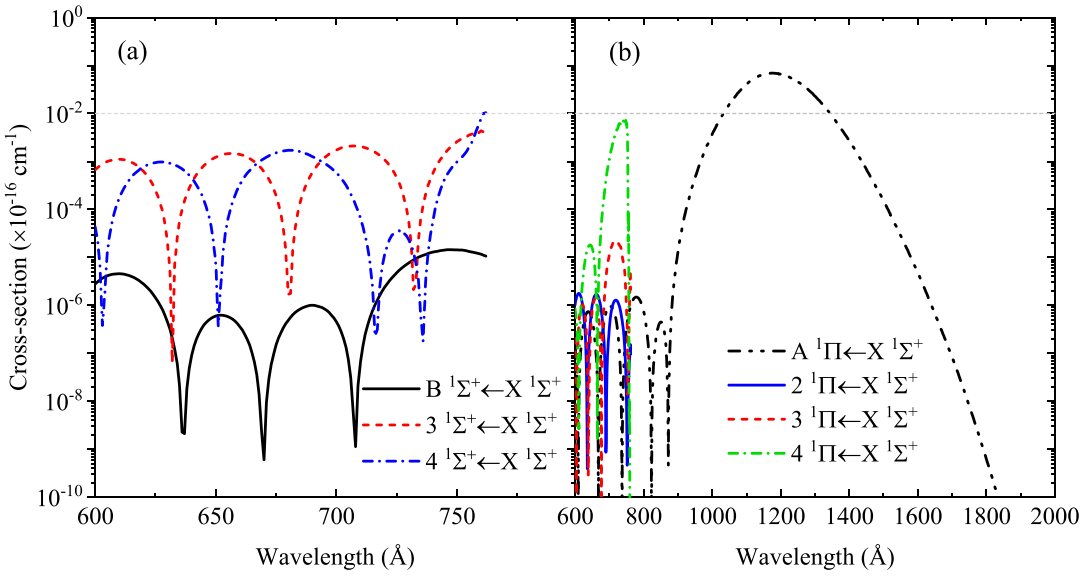

Figure 10. State-resolved photodissociation cross sections for seven electronic transitions of HF from the ground rovibrational level $(\upsilon'', J'') = (0, 0)$.

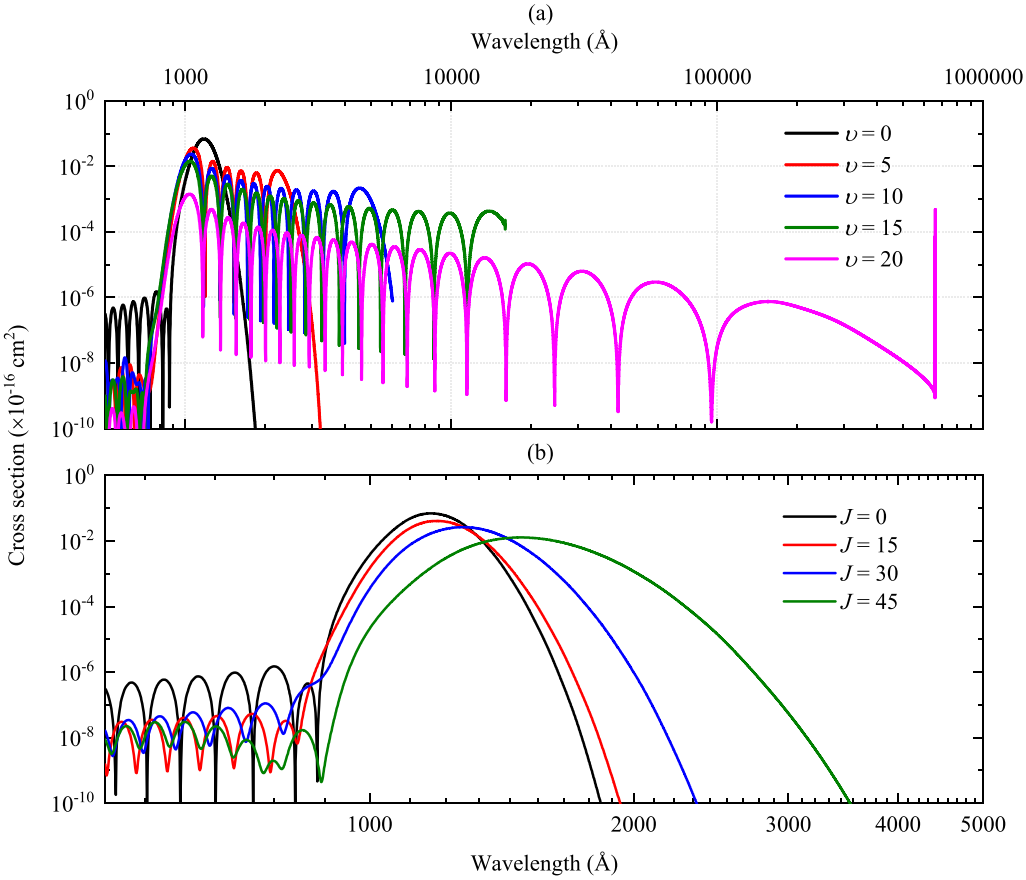

Figure 11. The computed state-resolved photodissociation cross sections of HF for the A $^1\Pi \leftarrow$X $^1\Sigma^+$ transition from initial rovibrational levels (a) where $J'' = 0$ and $\upsilon'' = 0$, 5, 10, 15, and 20 and (b) where $\upsilon'' = 0$ and $J'' = 0$, 15, 30, and 45.

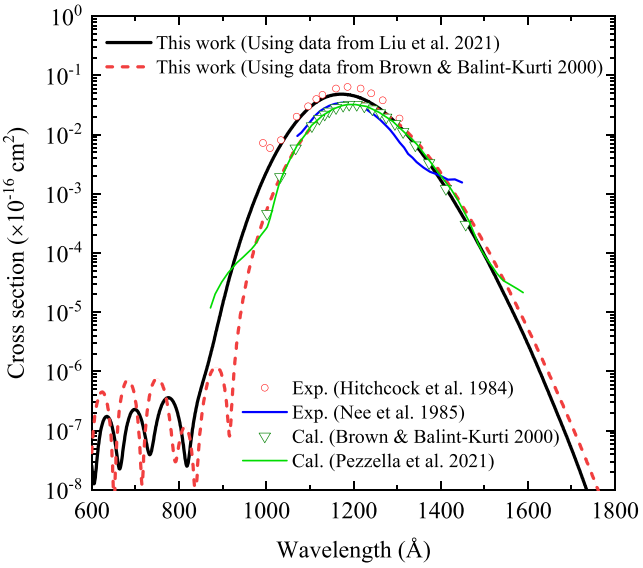

Figure 12. Comparison of the photodissociation cross sections of HF A $^1\Pi \leftarrow$X $^1\Sigma^+$ transition with experimental data from Hitchcock et al. (1984) and Nee et al. (1985) and the calculational results from Brown & Balint-Kurti (2000a) and Pezzella et al. (2021). Our photodissociation cross sections are obtained at 100 K.

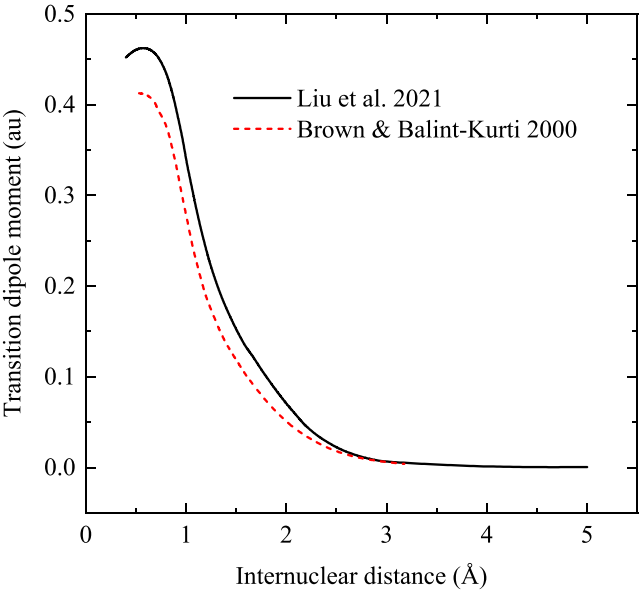

Figure 13. Transition dipole moments of the HF A $^1\Pi \leftarrow$X $^1\Sigma^+$ transition from Liu et al. (2021) and Brown & Balint-Kurti (2000a).

considered for exploring possible and important photodissociation transition channels.

3.1 HCl

State-resolved photodissociation cross sections of HCl have been computed for nine transitions from 871 rovibrational levels of the X $^1\Sigma^+$ state to the excited 2 $^1\Sigma^+$, 3 $^1\Sigma^+$, 4 $^1\Sigma^+$, A $^1\Pi$, 2 $^1\Pi$, 3 $^1\Pi$, 4 $^1\Pi$, 5 $^1\Pi$, and 6 $^1\Pi$ states. Cross sections are computed as a function of wavelength from 500 Å to the relevant threshold or 100 000 Å in 1 Å increment. Fig. 3 exhibits the state-resolved cross sections for each transition from the ground rovibrational level (υ'', J'') = (0, 0). As shown, the A $^1\Pi \leftarrow$X $^1\Sigma^+$ transition contributes most from the ground rovibrational levels and its maximum cross section is about four orders of magnitude larger than that of other electronic transitions. One of the reasons may be that the A $^1\Pi$ state is totally repulsive and all the A $^1\Pi \leftarrow$X $^1\Sigma^+$ transition probabilities lie in the rovibrational continuum. The threshold for ground-state photodissociation through the A $^1\Pi$ state occurs at 2831 Å, producing H (^2S_g) and Cl (^2P_u) atoms. A sample of the cross sections of the A $^1\Pi \leftarrow$X $^1\Sigma^+$ transition is displayed in Fig. 4 for several vibrational levels ($\upsilon'' = 0$, 5, 10, 15, and 20) at their corresponding lowest rotational level $J'' = 0$ and for several rotational levels ($J'' = 0$, 15, 30, and 45) in their ground vibrational level $\upsilon'' = 0$.

Based on the state-resolved cross sections, LTE cross sections have been computed for each transition from 0 to 10 000 K. For the A $^1\Pi \leftarrow$X $^1\Sigma^+$ transition, its photodissociation cross section at 100 K is shown in Fig. 5, compared to previous experiments (Inn 1975; Nee et al.1986; Cheng et al. 2002) and theoretical calculations (van Dishoeck et al.1982; Pezzella et al. 2021). The maximum value of the photodissociation cross section σ_{max} of the A $^1\Pi \leftarrow$X $^1\Sigma^+$ transition is calculated to be 3.34 × 10^{-8} cm^2, which is very close to the experimental values of 3.82 × 10^{-8} cm^2 from Inn (1975) with the uncertainty of ±0.38 × 10^{-8} cm^2, and of 3.28 × 10^{-8} cm^2 from Nee et al. (1986) with the uncertainty of ±0.49 × 10^{-8} cm^2, and of 3.53 × 10^{-8} cm^2 from Cheng et al. (2002) with the uncertainty of ±0.18 × 10^{-8} cm^2. The peak position λ_{max} is estimated to be 1549 Å, which is slightly (about 1 nm) larger than that obtained in the experiments and slightly smaller (about 2 nm) than that in the previous calculations. For wavelengths larger than λ_{max}, our results show good agreement with the experiments and the calculational ones by van Dishoeck et al. (1982), but smaller than those computed by Pezzella et al. (2021). For wavelengths smaller than λ_{max}, our photodissociation cross sections are in good agreement with those computed by Pezzella et al. (2021), while both theoretical calculations underestimate the cross sections relative to the experiments. Also, the computational cross sections of van Dishoeck et al. (1982) are smaller than those obtained in the experiments and calculations from this work and Pezzella et al. (2021). Overall, our photodissociation cross section of the A $^1\Pi \leftarrow$X $^1\Sigma^+$ is reliable.

Photodissociation cross sections of nine electronic transitions for HCl at 0 K are presented in Fig. 6. The discrete transitions for the 2 $^1\Sigma^+ \leftarrow$X $^1\Sigma^+$, 3 $^1\Sigma^+ \leftarrow$X $^1\Sigma^+$, 4 $^1\Sigma^+ \leftarrow$X $^1\Sigma^+$, 2 $^1\Pi \leftarrow$X $^1\Sigma^+$, 3 $^1\Pi \leftarrow$X $^1\Sigma^+$, 4 $^1\Pi \leftarrow$X $^1\Sigma^+$, 5 $^1\Pi \leftarrow$X $^1\Sigma^+$, and 6 $^1\Pi \leftarrow$X $^1\Sigma^+$ transitions are calculated using the DUO and EXOCROSS programs (Yurchenko et al. 2016; Yurchenko, Al-Refaie & Tennyson 2018) and smoothed using the method provided by the ExoMol group (Pezzella et al. 2021, 2022), i.e. a normalized Gaussian function. These spectra are compared with the Leiden Observatory database (Heays et al. 2017), which result from the combination of a direct measurement (Bahou et al. 2001) and electron-energy-loss spectroscopy (Brion et al. 2005). The total spectrum is mainly composed of a continuum band of the A $^1\Pi \leftarrow$X $^1\Sigma^+$ transition and discrete progressions of the 2 $^1\Pi \leftarrow$X $^1\Sigma^+$, 3 $^1\Sigma^+ \leftarrow$X $^1\Sigma^+$, 4 $^1\Sigma^+ \leftarrow$X $^1\Sigma^+$, 4 $^1\Pi \leftarrow$X $^1\Sigma^+$, and 6 $^1\Pi \leftarrow$X $^1\Sigma^+$ transitions. The contributions of the discrete 2 $^1\Sigma^+ \leftarrow$X $^1\Sigma^+$, 3 $^1\Pi \leftarrow$X $^1\Sigma^+$, and 5 $^1\Pi \leftarrow$X $^1\Sigma^+$ transitions are relatively small. As shown in Fig. 6, the total spectrum is in reasonable agreement with that from the Leiden Observatory database. The cross sections below about 1040 Å are not produced in this work and are expected to result from the photodissociation to higher electronic states or predissociation via spin–orbit couplings.

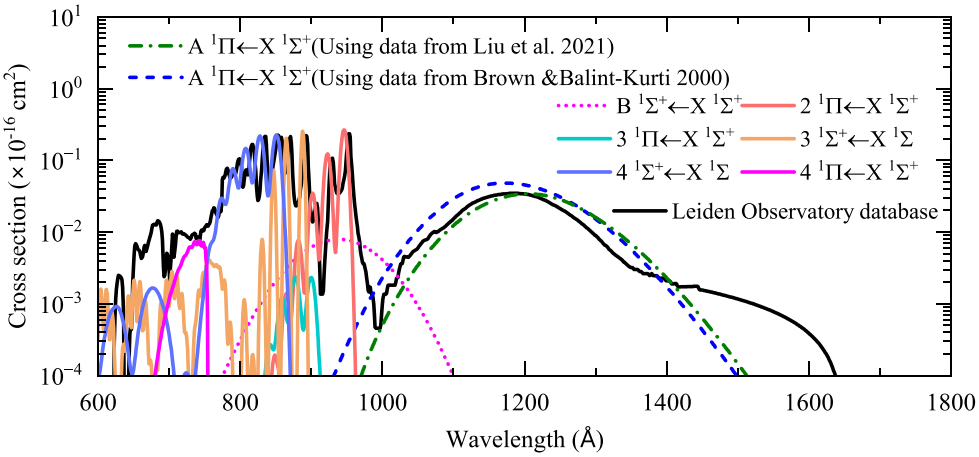

Figure 14. Photodissociation cross sections of HF for seven electronic transitions at 0 K. The total spectrum is composed of a continuum band of the A $^1\Pi\leftarrow X\ ^1\Sigma^+$ transition at wavelengths larger than about 1010 Å, a discrete progression of 2 $^1\Pi\leftarrow X\ ^1\Sigma^+$ at wavelengths about 900–960 Å, a discrete progression of 3 $^1\Sigma^+\leftarrow X\ ^1\Sigma^+$ at wavelengths about 860–900 Å, a discrete progression of 3 $^1\Sigma^+\leftarrow X\ ^1\Sigma^+$ at wavelengths about 760–860 Å, and a continuum band of 4 $^1\Pi\leftarrow X\ ^1\Sigma^+$ at wavelength about 743 Å. Note that the peaks of discrete transitions depend greatly on the Gaussian smoothing function, while the integrated cross sections are conserved. The total cross sections are compared with the experimental data collected in Leiden Observatory database (Heays et al. 2017).

The total photodissociation cross sections of HCl at temperatures of 0, 500, 3000, and 10 000 K are presented in Fig. 7 and compared with those computed by the ExoMol group (Pezzella et al. 2022). As shown, our cross sections below $T = 3000$ K are in good agreement with the ExoMol's results over the entire wavelength range except for a short waveband near 1400 Å. The differences between two results even extend to larger wavelengths at $T = 10\,000$ K. Careful analyses show that these differences result from the different cross section of the 2 $^1\Sigma^+\leftarrow X\ ^1\Sigma^+$ transition. Although the TDM for 2 $^1\Sigma^+\leftarrow X\ ^1\Sigma^+$ is from the same paper of Engin et al. (2012) in our and ExoMol's studies, the selected values of the TDM at the equilibrium internuclear distance (R_e) are different. Pezzella et al. (2022) adopted the value in table IV from the paper of Engin et al. (2012), while we extracted the value from their fig. 3. The TDM of 2 $^1\Sigma^+\leftarrow X\ ^1\Sigma^+$ at R_e is 0.4411 au in their table IV, which is quite different from that given in their fig. 3. Also, the TDM of 2 $^1\Sigma^+\leftarrow X\ ^1\Sigma^+$ at R_e is the same as that of 3 $^1\Sigma^+\leftarrow X\ ^1\Sigma^+$ in their table IV. Therefore, we deduce that the TDM of 2 $^1\Sigma^+\leftarrow X\ ^1\Sigma^+$ at R_e in their table IV may be a typographical error. Hence, we carried out an *ab initio* calculation of the TDM for 2 $^1\Sigma^+\leftarrow X\ ^1\Sigma^+$ using the MRCI+Q method with the aug-cc-pCV5Z-DK basis set for Cl and the aug-cc-pV5Z-DK basis set for H. The result is displayed in Fig. 8, along with the values given by Engin et al. (2012). As shown, our deduction is correct.

Photodissociation rates of HCl are then computed using the LTE cross sections by considering the interstellar and blackbody radiation fields. Photodissociation rates for each transition in the ISRF are presented in Table 1. The total photodissociation rate of HCl in the ISRF increases by a factor of 1.2 as the temperature increases from 0 to 10 000 K. The total photodissociation rate at 0 K is 1.10×10^{-9} s^{-1}, which is larger than that of 9.81×10^{-10} s^{-1} computed by van Dishoeck et al. (1982), because we consider more excited states. Although we consider the same electronic transitions as those given by Pezzella et al. (2022), our total photodissociation rate is lower than that of 1.23×10^{-9} s^{-1} calculated by Pezzella et al. (2022). The difference results from the different treatment of the 2 $^1\Sigma^+\leftarrow X\ ^1\Sigma^+$ transition. The computed rates of the A $^1\Pi\leftarrow X\ ^1\Sigma^+$ and 2 $^1\Pi\leftarrow X\ ^1\Sigma^+$ transitions are 2.1×10^{-10} and 5.1×10^{-10} s^{-1}, respectively, which are very close to those of 2.1×10^{-10} and 5.3×10^{-10} s^{-1} estimated by van Dishoeck et al. (1982) and those of 2.3×10^{-10} and 5.2×10^{-10} s^{-1} calculated by Pezzella et al. (2022). Note that the total photodissociation rate of HCl is lower than that of 1.7×10^{-9} s^{-1} presented by Heays et al. (2017), because we do not consider the cross sections below about 1040 Å. The photodissociation rates in blackbody radiation fields of 4000, 10 000, and 20 000 K are displayed in Fig. 9. The results show similar trend as those reported by Pezzella et al. (2022). The total rates for the blackbodies of 4000, 10 000, and 20 000 K are 1.06×10^{-10}, 4.51×10^{-10}, and 9.29×10^{-10} s^{-1} versus 9.35×10^{-11}, 5.06×10^{-10}, and 1.47×10^{-9} s^{-1} presented by Heays et al. (2017), and 1.43×10^{-10}, 5.36×10^{-10}, and 1.06×10^{-9} s^{-1} computed by Pezzella et al. (2022).

3.2 HF

As above, we first compute the state-resolved photodissociation cross sections of HF, which have been investigated for the B $^1\Sigma^+\leftarrow X\ ^1\Sigma^+$, 3 $^1\Sigma^+\leftarrow X\ ^1\Sigma^+$, 4 $^1\Sigma^+\leftarrow X\ ^1\Sigma^+$, A $^1\Pi\leftarrow X\ ^1\Sigma^+$, 2 $^1\Pi\leftarrow X\ ^1\Sigma^+$, 3 $^1\Pi\leftarrow X\ ^1\Sigma^+$, and 4 $^1\Pi\leftarrow X\ ^1\Sigma^+$ transitions where 871 rovibrational levels of the ground state are considered and the wavelengths cover from 500 Å to the related threshold or 100 000 Å. Fig. 10 shows the state-resolved photodissociation cross sections for seven electronic transitions mentioned above from the rovibrational level $(\upsilon'', J'') = (0, 0)$ of the X $^1\Sigma^+$ state. The A $^1\Pi\leftarrow X\ ^1\Sigma^+$ transition covers a relatively large wavelength range up to 2043 Å. We presented a sample of the state-resolved cross sections of the A $^1\Pi\leftarrow X\ ^1\Sigma^+$ transition in Fig. 11 by varying the vibrational levels for $J = 0$ and by changing rotational levels for $\upsilon = 0$.

Using the state-resolved cross sections, LTE cross sections have been computed for the considered seven transitions of HF at temperatures from 0 to 10 000 K. The cross section for the A $^1\Pi\leftarrow X\ ^1\Sigma^+$ transition at 100 K is displayed in Fig. 12. Our cross section is between the electron energy-loss spectra measured by Hitchcock et al. (1984) and the synchrotron spectra measured by Nee et al. (1985). The maximum of the cross section σ_{max} is about the average of two experimental σ_{max} values. While the theoretical results of Brown & Balint-Kurti (2000a) and Pezzella et al. (2021) are very close to the synchrotron spectra measured by Nee et al. (1985). The experimental

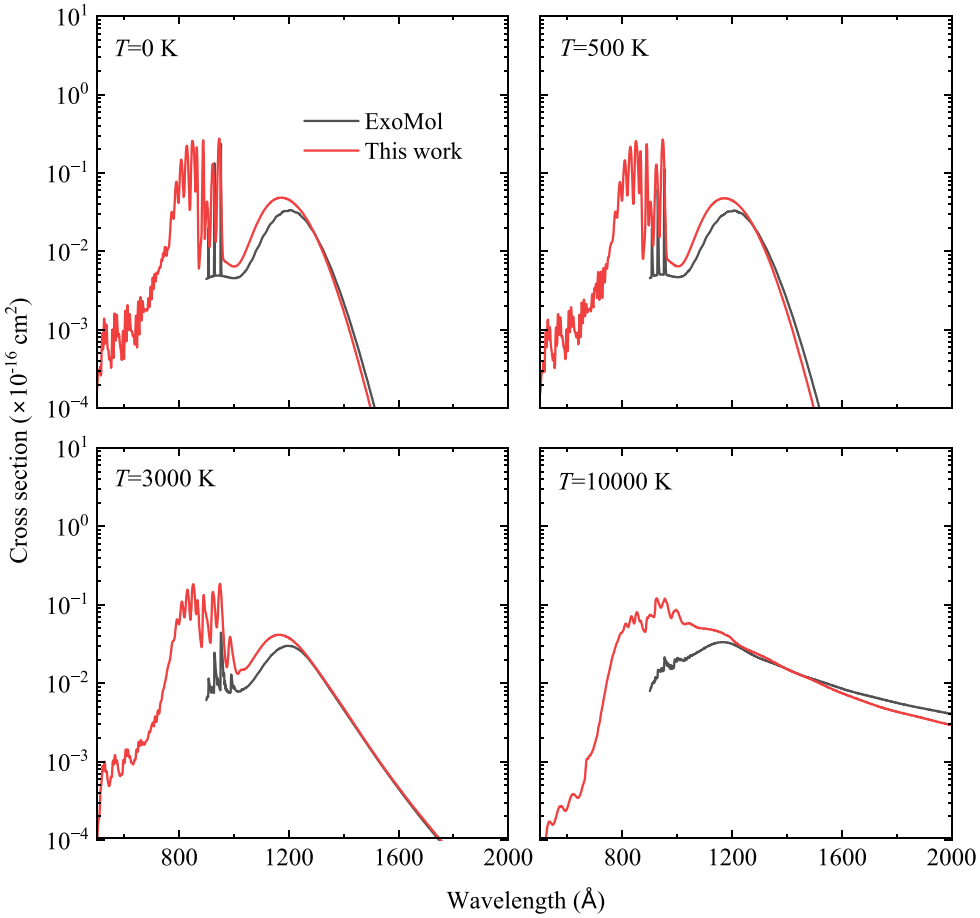

Figure 15. Comparison of the total photodissociation cross section of HF with that from ExoMol group (Pezzella et al. 2022).

Table 2. Photodissociation rates (s^{-1}) of HF under the standard ISRF at several temperatures.

	0 K	500 K	1000 K	2000 K	3000 K	5000 K	10 000 K
B $^1\Sigma^+ \leftarrow$X $^1\Sigma^+$	5.14×10^{-12}	5.36×10^{-12}	5.75×10^{-12}	8.57×10^{-12}	1.52×10^{-11}	4.19×10^{-11}	1.80×10^{-10}
3 $^1\Sigma^+ \leftarrow$X $^1\Sigma^+$	2.56×10^{-36}	2.05×10^{-16}	6.53×10^{-14}	1.29×10^{-12}	3.90×10^{-12}	1.08×10^{-11}	2.79×10^{-11}
4 $^1\Sigma^+ \leftarrow$X $^1\Sigma^+$	4.73×10^{-62}	4.15×10^{-23}	3.01×10^{-18}	8.61×10^{-16}	6.54×10^{-15}	4.53×10^{-14}	3.52×10^{-13}
A $^1\Pi \leftarrow$X $^1\Sigma^+$	1.73×10^{-10}	1.70×10^{-10}	1.69×10^{-10}	1.67×10^{-10}	1.65×10^{-10}	1.58×10^{-10}	1.37×10^{-10}
2 $^1\Pi \leftarrow$X $^1\Sigma^+$	1.94×10^{-11}	1.97×10^{-11}	2.01×10^{-11}	2.15×10^{-11}	2.38×10^{-11}	2.98×10^{-11}	4.66×10^{-11}
3 $^1\Pi \leftarrow$X $^1\Sigma^+$	1.06×10^{-15}	1.55×10^{-15}	2.94×10^{-15}	1.17×10^{-14}	2.99×10^{-14}	1.68×10^{-13}	3.85×10^{-12}
4 $^1\Pi \leftarrow$X $^1\Sigma^+$	4.19×10^{-154}	3.35×10^{-39}	1.04×10^{-25}	1.02×10^{-18}	3.36×10^{-16}	5.46×10^{-14}	2.98×10^{-12}
Total	1.98×10^{-10}	1.95×10^{-10}	1.95×10^{-10}	1.98×10^{-10}	2.08×10^{-10}	2.41×10^{-10}	3.99×10^{-10}

data of Nee et al. (1985) are a factor of 2 smaller than those obtained by Hitchcock et al. (1984) and there seems no criterion to check which is more reliable. Further analyses indicate that the differences between our cross sections and previous calculational ones (Brown & Balint-Kurti 2000a; Pezzella et al. 2021) may come from different data sources of PECs and TDMs. Therefore, the PECs and TDM from Brown & Balint-Kurti (2000a), which are also used by Pezzella et al. (2021), are adopted to compute the LTE cross sections of the HF $A^1\Pi \leftarrow X^1\Sigma^+$ transition. The results are in good agreement with previous calculations (as shown in Fig. 12), which has confirmed our guess.

Further analyses found that the differences of different theoretical cross sections mainly resulted from the two different sets of TDM, as shown in Fig. 13. The TDM of Liu et al. (2021) is larger than that obtained by Brown & Balint-Kurti (2000a). Liu et al. (2021) and Brown & Balint-Kurti (2000a) both used the MRCI method, but selected different basis sets. Liu et al. (2021) had made a critical evaluation of the effect of different basis sets on the energy levels of the F and H atoms. By comparing with the experimental energy levels, they adopted the optimum basis set for the calculation of the PECs and TDMs, i.e. the aug-cc-pV5Z+2s2p2d and d-aug-cc-pV5Z+1s2p2d1f basis sets are chosen for F and H atom, respectively. While Brown & Balint-Kurti (2000a) utilized the aug-cc-pV5Z basis set. Therefore, the TDM of HF $A\,^1\Pi \leftarrow X\,^1\Sigma^+$ from Liu et al. (2021) is more reliable in theory. In addition, there has already existed the cross section of HF A $^1\Pi \leftarrow$X $^1\Sigma^+$ based on *ab initio* data

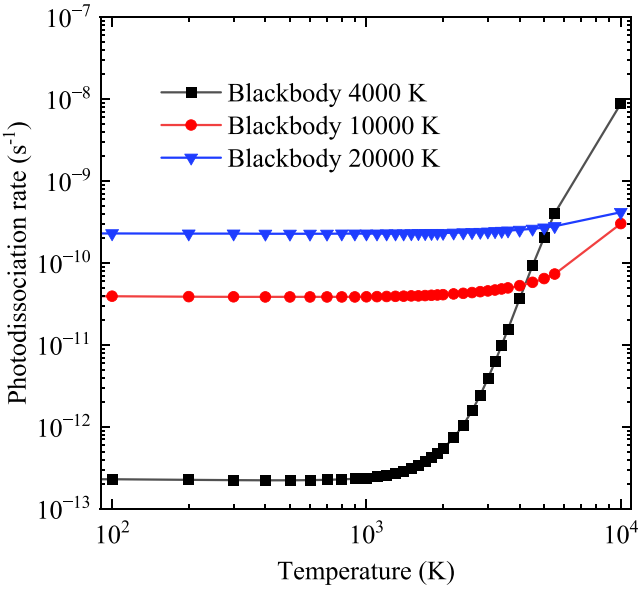

Figure 16. Photodissociation rates of HF in the blackbody radiation fields of 4000 K (in black), 10 000 K (in red), and 20 000 K (in blue). The blackbody of 4000 K increases the rate by three orders of magnitude from 100 to 10 000 K. The rates obtained using the blackbodies of 10 000 and 20 000 K do not show significant change, with factors of 7.7 and 1.8, respectively.

from Brown & Balint-Kurti (2000a), so we adopted a different *ab initio* data from Liu et al. (2021) to perform the computation of subsequent photodissociation cross sections and rates for guiding possible experiments in the future.

Photodissociation cross sections of nine electronic transitions for HF at 0 K are presented in Fig. 14. The discrete transitions of B $^1\Sigma^+\leftarrow$X $^1\Sigma^+$, 3 $^1\Sigma^+\leftarrow$X $^1\Sigma^+$, 4 $^1\Sigma^+\leftarrow$X $^1\Sigma^+$, 2 $^1\Pi\leftarrow$X $^1\Sigma^+$, and 3 $^1\Pi\leftarrow$X $^1\Sigma^+$ for HF are treated using the same method as HCl. These spectra are compared with the Leiden Observatory database (Heays et al. 2017), which results from the vacuum UV photoabsorption spectrum measured by electron-energy-loss spectroscopy (Hitchcock et al. 1984), but with a factor of 0.53 to match the experimental cross section of A $^1\Pi\leftarrow$X $^1\Sigma^+$ from Nee et al. (1985). Related discussions about these two experiments are given above. The total cross section is composed of a continuum band of the A $^1\Pi\leftarrow$X $^1\Sigma^+$ transition, a continuum band of the 4 $^1\Pi\leftarrow$X $^1\Sigma^+$ transition, and discrete progressions of the 2 $^1\Pi\leftarrow$X $^1\Sigma^+$, 3 $^1\Sigma^+\leftarrow$X $^1\Sigma^+$, and 4 $^1\Sigma^+\leftarrow$X $^1\Sigma^+$ transitions. As shown in Fig. 14, the total cross section agrees well with that from the Leiden Observatory database.

The total photodissociation cross sections of HF at temperatures of 0, 500, 3000, and 10 000 K are presented in Fig. 15 and compared with those computed by the ExoMol group (Pezzella et al. 2022). Except for the A $^1\Pi\leftarrow$X $^1\Sigma^+$, B $^1\Sigma^+\leftarrow$X $^1\Sigma^+$, and 2 $^1\Pi\leftarrow$X $^1\Sigma^+$ transitions considered by the ExoMol group, we have also studied the cross sections of the discrete 3 $^1\Sigma^+\leftarrow$X $^1\Sigma^+$, 4 $^1\Sigma^+\leftarrow$X $^1\Sigma^+$, 3 $^1\Pi\leftarrow$X $^1\Sigma^+$, and 4 $^1\Pi\leftarrow$X $^1\Sigma^+$ transitions, which contribute to the wavelengths below about 900 Å. Moreover, a different set of cross section of the A $^1\Pi\leftarrow$X $^1\Sigma^+$ transition is computed based on the recent *ab initio* data from Liu et al. (2021). The maximum of the cross section $\sigma_{\max}$ is about 1.44 times that from the ExoMol's result.

Photodissociation rates of HF are then obtained by considering the interstellar and blackbody radiation fields. Photodissociation rates for each transition in the ISRF are presented in Table 2. The total photodissociation rate of HF in the ISRF increases by a factor of 2 as the temperature increases from 0 to 10 000 K. For the A $^1\Pi\leftarrow$X $^1\Sigma^+$ transition, our calculation using PECs and TDMs of Liu et al. (2021) estimates a photodissociation rate of 1.73×10^{-10} s^{-1} (at 0 K), which is approximately 1.5 times than that obtained using PECs and TDMs of Brown & Balint-Kurti (2000a). For the 3 $^1\Sigma^+\leftarrow$X $^1\Sigma^+$, 4 $^1\Sigma^+\leftarrow$X $^1\Sigma^+$, 3 $^1\Pi\leftarrow$X $^1\Sigma^+$, and 4 $^1\Pi\leftarrow$X $^1\Sigma^+$ transitions, the cross sections contribute little in the wavelengths of ISRF and their contributions to the ISRF rate increase with the increasing temperature. In the blackbody radiation fields of 4000, 10 000, and 20 000 K, photodissociation rates of HF are estimated and presented in Fig. 16. The variation trend is in good agreement with that reported by Pezzella et al. (2022). The total rates for the blackbodies of 4000, 10 000, and 20 000 K are 2.30×10^{-13}, 3.93×10^{-11}, and 2.29×10^{-10} s^{-1} versus 5.31×10^{-13}, 2.88×10^{-11}, and 1.17×10^{-10} s^{-1} presented by Heays et al. (2017), and 3.37×10^{-13}, 3.24×10^{-11}, and 1.38×10^{-10} s^{-1} computed by Pezzella et al. (2022).

4 CONCLUSIONS

In this work, we have performed an *ab initio* investigation of the ground-state photodissociation of HCl and HF via several excited states. The state-resolved cross sections and temperature-dependent LTE cross sections have been computed for the electronic transitions of HCl and HF from all the rovibrational levels of their ground states. The considered wavelengths cover from 500 Å to the threshold or 100 000 Å. The cross sections are then used to compute the photodissociation rates in the interstellar and blackbody radiation fields. The photodissociation cross sections and rates for different electronic and rovibrational transitions are discussed in details and can be used for chemical modelling in astrophysical environments, such as in the interstellar medium and in the atmospheres of Venus and hot exoplanets.

The computed cross section of the A $^1\Pi\leftarrow$X $^1\Sigma^+$ transition for HCl agrees well with previous theoretical and experimental values. However, for HF, the cross section of its A $^1\Pi\leftarrow$X $^1\Sigma^+$ transition is undecidable and greatly depends on the selected PECs and TDMs. The latest PECs and TDMs from Liu et al. (2021) produce the cross sections between the experimental ones from Hitchcock et al. (1984) and those observed by Nee et al. (1985). The maximum of the cross section $\sigma_{\max}$ is about the average of two experimental $\sigma_{\max}$ values. While the PECs and TDMs from Brown & Balint-Kurti (2000a) lead to the cross sections in very good agreement with those measured by Nee et al. (1985). Further analyses show that such difference mainly results from the different theoretical values of TDMs. No explicit statements are found to judge the accuracy of two experimental sources of the A $^1\Pi\leftarrow$X $^1\Sigma^+$ cross sections. The theoretical sources of PECs and TDMs cannot also determine which experiment is more accurate. As such, we strongly encourage further experimental study of the A $^1\Pi\leftarrow$X $^1\Sigma^+$ transition for HF to give a definite guideline for its cross sections.

More recently, the ExoMol group just provided a very similar study of the photodissociation cross sections and rates of HCl and HF (Pezzella et al. 2022). We made careful comparisons with their results. Overall, our results are in good agreement with those provided by the ExoMol group. There exist some differences in the treatment of these two molecular systems. For HCl, we adopted different value of TDM at R_e in dealing with the 2 $^1\Sigma^+\leftarrow$X $^1\Sigma^+$ transition. For HF, we provided a different photodissociation cross section of the A $^1\Pi\leftarrow$X $^1\Sigma^+$ transition by using a recent *ab initio* PECs and TDM for the X $^1\Sigma^+$ and A $^1\Pi$ states (Liu et al. 2021). We also added the 3 $^1\Sigma^+\leftarrow$X $^1\Sigma^+$, 4 $^1\Sigma^+\leftarrow$X $^1\Sigma^+$, 3 $^1\Pi\leftarrow$X $^1\Sigma^+$,

and $4\,^1\Pi \leftarrow X\,^1\Sigma^+$ transitions, whose cross sections are dominant at wavelengths below about 900 Å. In addition, our photodissociation cross sections and rates agree reasonably with those reported in the Leiden Observatory database (Heays et al. 2017).

ACKNOWLEDGEMENTS

We thank Selma Engin and Bing Yan for providing *ab initio* data of HCl and HF, respectively. This work is supported by National Natural Science Foundation of China (52106098, 51421063). ZQ acknowledges the support from Natural Science Foundation of Shandong Province (ZR2021QE021), China Postdoctoral Science Foundation (2021M701977), Postdoctoral Innovation Project of Shandong Province, and Postdoctoral Applied Research Project of Qingdao City. The scientific calculations in this paper have been done on the HPC Cloud Platform of Shandong University.

CONFLICT OF INTEREST

There are no conflicts to decare.

DATA AVAILABILITY

The PECs and TDMs of HCl and HF are provided in the Supplementary Material, along with the temperature-dependent photodissociation cross sections of HCl and HF. The reporting temperatures are provided according to those given by the ExoMol group. The cross sections can also be obtained online at https://dr-zhi-qin.github.io/personal/Database.html.

REFERENCES

Appenzeller I., Mundt R., 1989, A&AR, 1, 291
Bahou M., Chung C.-Y., Lee Y.-P., Cheng B.-M., Yung Y. L., Lee L. C., 2001, ApJ, 559, L179
Bai T., Qin Z., Liu L., 2021, MNRAS, 505, 2177
Bai T., Qin Z., Liu L., 2022, MNRAS, 510, 1649
Brion C. E., Dyck M., Cooper G., 2005, J. Electron Spectrosc. Related Phenomena, 144, 127
Brown A., Balint-Kurti G. G., 2000a, J. Chem. Phys., 113, 1870
Brown A., Balint-Kurti G. G., 2000b, J. Chem. Phys., 113, 1879
Cacelli I., 1996, Chem. Phys. Lett., 249, 149
Cheng B.-M., Chung C.-Y., Bahou M., Lee Y.-P., Lee L. C., 2002, J. Chem. Phys., 117, 4293
De Keyser J. et al., 2017, MNRAS, 469, S695
Dhooghe F. et al., 2017, MNRAS, 472, 1336
el-Qadi W. H., Stancil P. C., 2013, ApJ, 779, 97
Engin S., Sisourat N., Carniato S., 2012, J. Chem. Phys., 137, 154304
Grebenshchikov S. Y., 2016, J. CO2 Utilization, 15, 32
Habets G. M. H. J., Heintze J. R. W., 1981, A&AS, 46, 193
Hansson A., Watson J. K. G., 2005, J. Mol. Spectrosc., 233, 169
Heays A. N., Bosman A. D., van Dishoeck E. F., 2017, A&A, 602, A105
Hitchcock A. P., Williams G. R. J., Brion C. E., Langhoff P. W., 1984, Chem. Phys., 88, 65
Indriolo N., Neufeld D. A., Seifahrt A., Richter M. J., 2013, ApJ, 764, 188
Inn E. C. Y., 1975, J. Atmos. Sci., 32, 2375
Johnson B. R., 1977, J. Chem. Phys., 67, 4086
Johnson B. R., 1978, J. Chem. Phys., 69, 4678
Kramida A., Ralchenko Y., Reader J., NIST ASD Team, 2021, NIST Atomic Spectra Database (version 5.9). National Institute of Standards and Technology, Gaithersburg, MD, a vailable at https://physics.nist.gov/asd
Liu Y., Sun Q., Liu Y., Xue J., Li R., Yan B., 2021, J. Quant. Spectrosc. Radiat. Transf., 271, 107737
London F., 1937, Trans. Faraday Soc., 33, 8b
McMillan E. C., Shen G., McCann J. F., McLaughlin B. M., Stancil P. C., 2016, J. Phys. B: At. Mol. Opt. Phys., 49, 084001
Miyake S., Gay C. D., Stancil P. C., 2011, ApJ, 735, 21
Monje R. R., Lis D. C., Roueff E., Gerin M., De Luca M., Neufeld D. A., Godard B., Phillips T. G., 2013, ApJ, 767, 81
Myer J. A., Samson J. A. R., 1970, J. Chem. Phys., 52, 266
Natta A., 1993, ApJ, 412, 761
Nee J. B., Suto M., Lee L. C., 1985, J. Phys. B: At. Mol. Opt. Phys., 18, L293
Nee J. B., Suto M., Lee L. C., 1986, J. Chem. Phys., 85, 719
Pezzella M., Yurchenko S. N., Tennyson J., 2021, Phys. Chem. Chem. Phys., 23, 16390
Pezzella M., Tennyson J., Yurchenko S. N., 2022, MNRAS, 514, 4413
Qin Z., Bai T., Liu L., 2021a, MNRAS, 507, 2930
Qin Z., Bai T., Liu L., 2021b, ApJ, 917, 87
Qin Z., Bai T., Liu L., 2021c, MNRAS, 508, 2848
Qin Z., Bai T., Liu L., 2022, MNRAS, 510, 3011
Sandor B. J., Clancy R. T., 2012, Icarus, 220, 618
Smith P. L., Yoshino K., Black J. H., Parkinson W. H., 1980, ApJ, 238, 874
Valiev R. R., Berezhnoy A. A., Gritsenko I. S., Merzlikin B. S., Cherepanov V. N., Kurten T., Wöhler C., 2020, A&A, 633, A39
van Dishoeck E. F., Black J., 1982, ApJ, 258, 533
van Dishoeck E. F., van Hemert M. C., Dalgarno A., 1982, J. Chem. Phys., 77, 3693
Vioque M., Oudmaijer R. D., Baines D., Mendigutía I., Pérez-Martínez R., 2018, A&A, 620, A128
Wang K., Wang X., Fan Z., Zhao H. Y., Miao L., Yin G. J., Moro R., Ma L., 2021, Eur. Phys. J. D, 75, 1
Watson J. K. G., 2008, J. Mol. Spectrosc., 252, 5
Yung Y. L., DeMore W. B., 1982, Icarus, 51, 199
Yurchenko S. N., Lodi L., Tennyson J., Stolyarov A. V., 2016, Comput. Phys. Commun., 202, 262
Yurchenko S. N., Al-Refaie A. F., Tennyson J., 2018, A&A, 614, A131

SUPPORTING INFORMATION

Supplementary data are available at *MNRAS* online.

Supplemental material.zip

Please note: Oxford University Press is not responsible for the content or functionality of any supporting materials supplied by the authors. Any queries (other than missing material) should be directed to the corresponding author for the article.

This paper has been typeset from a Microsoft Word file prepared by the author.